Smell Driven Navigation for Soft Robotic Arms

Artificial Nose and Control

Piqué, F.; Stella, F.; Hughes, Josie; Falotico, Egidio ; Della Santina, C.

DOI
10.1109/RoboSoft55895.2023.10122116

Publication date
2023

Document Version
Final published version

Published in
Proceedings of the IEEE International Conference on Soft Robotics, RoboSoft 2023

Smell Driven Navigation for Soft Robotic Arms: Artificial Nose and Control

Francesco Piqué, Francesco Stella, Josie Hughes, Egidio Falotico and Cosimo Della Santina

***Abstract*— Elephants and other animals heavily rely on the sense of smell to operate. Soft robots would also benefit from an artificial sense of smell, which could be helpful in typical soft robotic tasks such as search and rescue, pipe inspection, and all the tasks involving unstructured environments. This work proposes an artificial nose on a soft robotic arm that ensures separate smell concentration readings. We propose designing the nose to generate a one-to-one matching between the sensors' inputs and the actuators. This design choice allows us to implement a simple control strategy tailored to reach a dynamically varying smell in the environment, which we validate on a two-segment tendon-driven soft robotic arm equipped with the proposed artificial nose. We also propose and validate in simulation a control strategy for reaching tasks in the case of a stationary smell.**

I. INTRODUCTION

The birth and development of soft robotics is strongly tied to bio-inspiration and bio-mimicry [1], [2]. The capabilities of animals like the octopus or the elephant are facilitated by the softness of their bodies, and also by their senses which allow them to intelligently explore the environment and make internal models based on the sensory data. The elephant, for example, is known to heavily depend upon the sense of smell through its trunk for cognitive tasks [3]. Inspired by this, in this paper we introduce an artificial nose for a soft robotic arm. Equipping soft robots with artificial sensing is nowadays a thriving field of research [4]. Vision has been implemented both with cameras at the tip in an eye in hand fashion [5], [6], and with external cameras, whose frames are usually used as ground truth data for machine learning schemes. Self sensing, or proprioception, has been implemented with a variety of sensors either embedded [7], [8], [9], [10], placed at the robot's base [11], or on the robot's body as a skin [12]. Tactile sensing via soft skins [13] is also a well studied topic. Audio devices have also been integrated in to soft robotic systems [14].

This work was supported by the European Union's Horizon Europe Program in the framework of PROBOSCIS Project (GA No. 863212), Human Brain Project SGA3 (GA No.945539) and Project EMERGE (GA No. 101070918).

Francesco Piqué and Egidio Falotico are with The BioRobotics Institute, Scuola Superiore Sant'Anna, Pisa, Italy and with the Department of Excellence in Robotics and AI, Scuola Superiore Sant'Anna, Pisa, Italy (email:{francesco.pique, egidio.falotico}@santannapisa.it).

Francesco Stella is with CREATE Lab, EPFL, Lausanne, Switzerland and with the Department of Cognitive Robotics, Delft University of Technology, Delft, The Netherlands. (e-mail: francesco.stella@epfl.ch).

Josie Hughes is with CREATE Lab, EPFL, Lausanne, Switzerland. (e-mail: josie.hughes@epfl.ch).

Cosimo Della Santina is with the Department of Cognitive Robotics, Delft University of Technology, Delft, The Netherlands and with the Institute of Robotics and Mechatronics, German Aerospace Center (DLR), Wessling, Germany. (email:c.dellasantina@tudelft.nl).

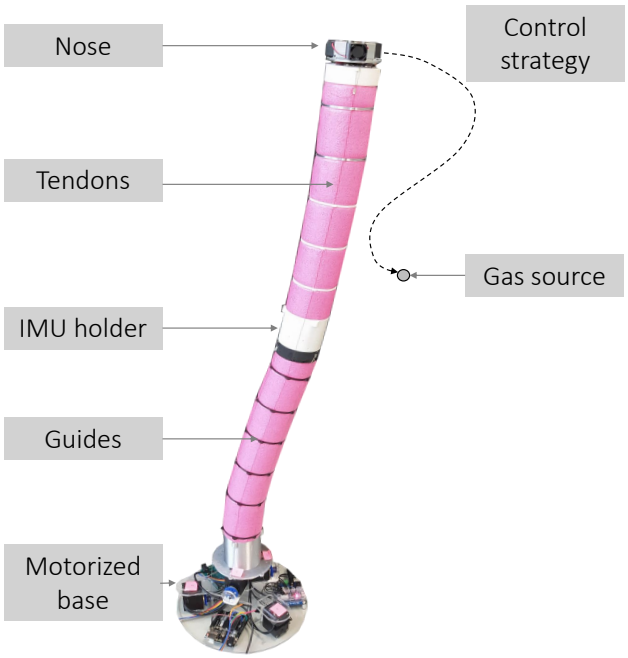

Fig. 1: The tendon driven soft arm used in this work, with the electronic nose placed on the tip. Thanks to a reduced model of the structure and the sensing on the tip, the soft manipulator is able to reach the source of signal.

However, out of the five senses, smell and taste have yet to be integrated into soft robotics. This paper concerns itself with the former, and its application to blind exploration. Outside of soft robotics, Persaud and Dodd [15] have first introduced the concept of "electronic nose". Using only two generic gas sensors, they could compare the ratios of the responses to different smells and gases and use such compared measures as an identifier for a specific odour. Later, electronic noses have been applied to navigation of mobile vehicles [16], [17], [18]. No examples exist of application to manipulators. With this work, we propose a nose design for applications in soft robotics, as shown in Fig. 1. The nose includes three sensors, this way allowing for directional sensing of odors. We align them with the typical topology of tendon driven soft robotic arms, so to pair each sensor with a tendon. We also propose two smell driven control strategies tailored for stationary or dynamic smells. The first is discussed in Sec. III and the second in Sec. IV. We validate the stationary one in simulation, leading to a precision in reaching a smell source of 5 % of the robot's length in average. We validate the second strategy with the platform shown in Fig. 1.

2023 IEEE International Conference on Soft Robotics (RoboSoft) | 979-8-3503-3222-3/23/$31.00 ©2023 IEEE | DOI: 10.1109/ROBOSOFT55895.2023.10122116

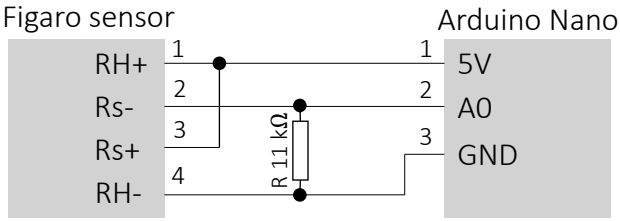

Fig. 2: The schematic of the wiring between a Figaro TGS-2600 gas sensor and the Arduino Nano.

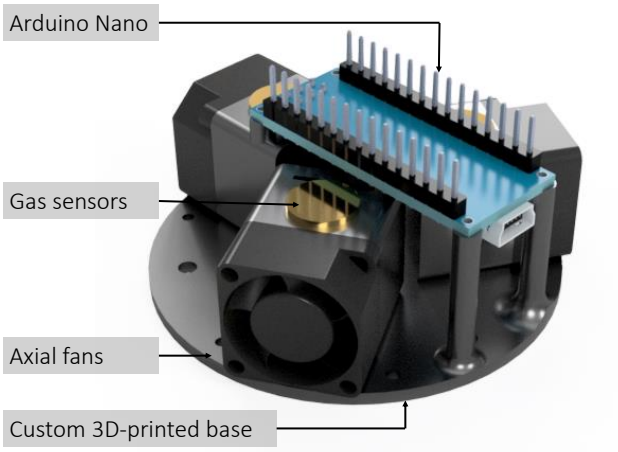

Fig. 3: The 3D CAD model of the custom designed holder for three gas sensors at a 120° angle and the Arduino Nano.

II. Hardware

After briefly introducing the two segment soft robot that we use in this work, we dive in the description of the proposed nose with directional sensing capabilities in II-B, and we validate its effectiveness with experiments in II-C.

A. Soft robot setup

A low cost, large scale, tendon driven soft arm has been built for this work. Its main body is made of two independently actuated segments made of a soft deformable foam (expanded polyethylene). On the tip and in the mid section Inertial Measurement Units (IMUs) have been placed so as to provide the orientation data in real time [10] (Fig. 1). The cables providing power and connection to the IMUs and the gas sensors are hosted in a custom made hole along the center of the foam body. Six Dynamixel XM430-W210 motors placed at the base of the robot, three for each segment, actuate the tendons which are attached to the tip of each segment and are routed along the body of the robot through 3D-printed guides.

B. Electronic nose

The sense of smell in humans and animals relies on receptors sensible to volatile chemical compounds. Similarly, in this work a triplet of Figaro TGS-2600 gas sensors was used. The sensors are composed by a typology of metal oxide sensors based on tin oxide (SnO_2) which, if heated, is subject to decrease in resistance when exposed to various nocive gases such as methane, carbon monoxide, ethanol, iso-buthane and hydrogen. The sensors were placed on the tip of the soft robot by means of a custom holder, shown in Fig. 3. The holder is designed so that the sensors are placed symmetrically at a 120° angle, so that each sensor is pointed towards a different direction around the robot's tip. This geometry also reflects the configuration of the tendons which actuate the arm. Each sensor was placed in a semi-closed separate housing, so as to better differentiate the direction sensed by each sensor. In this way each sensor has its own directionality, and its information can be exploited to formulate an approximation of the local gradient of gas signal, and so derive a smell-driven robot controller. The housing also contributes to physically separate the sensors from each other so as to ensure that their measures are as independent as possible. In front of the opening of each housing a 5V Sunon axial fan was placed in order to create a flow of air from the surrounding environment to the sensing element, and out of the housing from a slit placed at the back. The fans ensure a larger range of action of the sensors. Moreover, they ensure a shorter recovery time of the sensors because the gas is allowed to flow freely out of the housing without stagnating around the sensor after the smell source is removed from the proximity of the robot [19]. The sensors are then wired to an Arduino Nano placed on top of the holder structure, which streams the sensor data via a USB cable placed in the hollow of the robot's body to a PC. The schematic of the sensing element is shown in Fig. 2. For each sensor, The 5 V of the Arduino powers a heating element, RH, and the sensing element R_s. A loading resistance of $R_\mathrm{L} = 11k\Omega$ is placed for readout between the analog output of the sensor and ground. The voltage over the loading resistor V_RL is read by the analog input of the Arduino, and the sensing element resistance can be derived with $R_\mathrm{s} = \frac{(5V - V_\mathrm{RL})}{V_\mathrm{RL}} R_\mathrm{L}$. Every sensor must be pre-heated before reaching its regime resistance. Such baseline resistance $R0$ is subject to variations in between sensors and is also related to temperature and humidity conditions. In Fig.5 it is shown the pre-heating phase of the three sensors. After about 15 minutes the baseline resistances are reached for each sensor. Notably each sensors reaches a different baseline resistance.

C. Experimental results

To characterize the response of each sensor a smell source was placed around the electronic nose at constant distance of 10 cm and removed after few seconds while the response of each sensor was recorded. The trial was repeated with the smell source directly in front of every sensor, and in a halfway position between every sensor couple, so as to span the sensing space all around the nose. A cotton swab imbued in ethanol was used as a smell source due to availability of ethanol and to its relative non-toxicity with respect to the other gases to which the sensor is sensitive to. During the experiment the axial fans were turned on to ensure air flow. The resistances of the sensors fall accordingly to the location of the smell source in Fig. 4 (a-f). When the smell

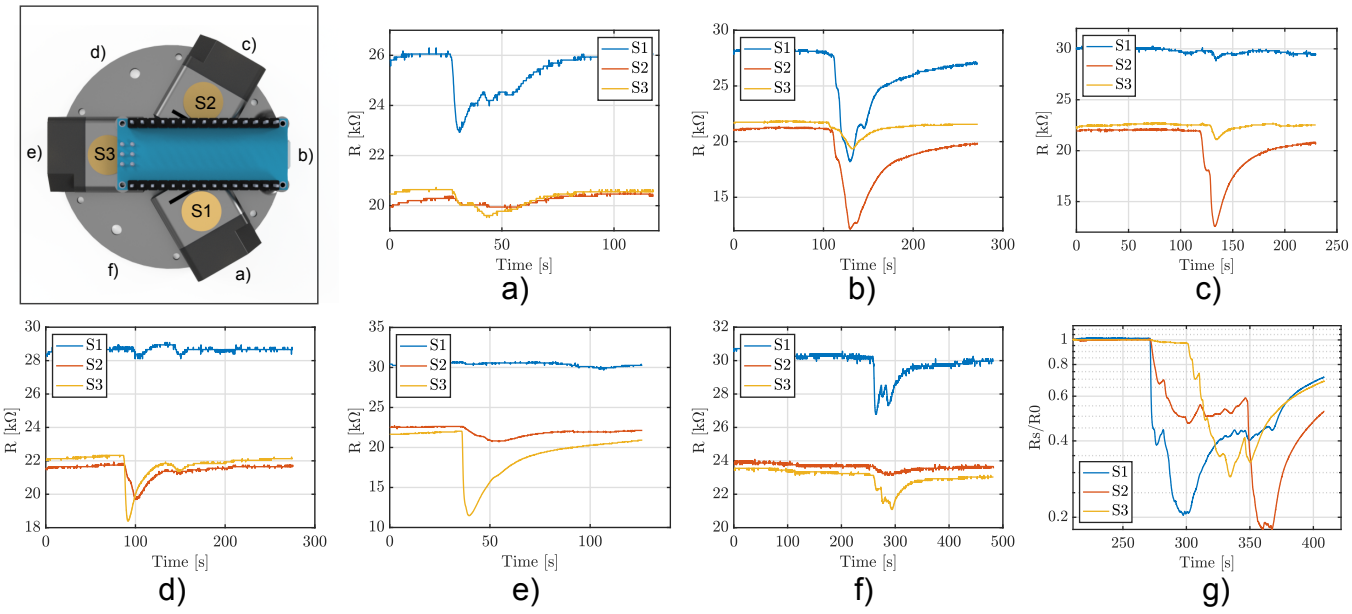

Fig. 4: Response of the electronic nose to smells placed at different orientations. In a),c),e) the smell is placed in front of sensor S1,S2,S3 respectively. In b),e),f) the smell is placed halfway in between sensors S1-S2, S2-S3 and S3-S1 respectively. In g) the response of the electronic nose to a smell placed sequentially in front of S1,S3,S2 without interrupting the trial is shown.

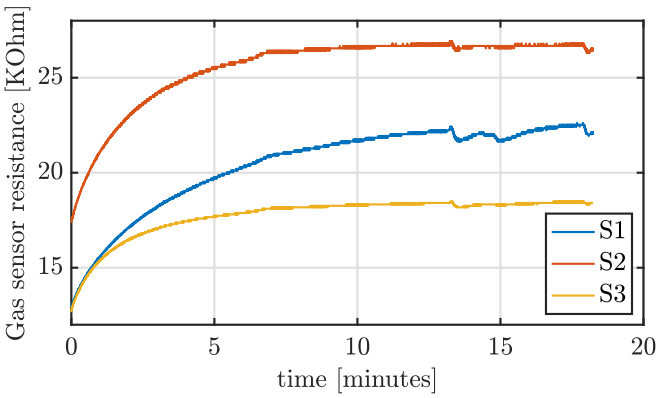

Fig. 5: Power up of the three gas sensors mounted on the tip of the soft robot. Note that each sensor reaches a different resistance baseline in about the same amount of time.

is placed in between two sensors the resistances of both the sensors decrease. A trial where the smell source is placed in front of each sensor sequentially was also performed and the response of the nose is shown in Fig. 4g. Here, we observe that, when the smell source is placed next to sensor S1, it's resistance normalized with respect to the baseline R0 falls immediately and faster than for sensor S2. Then, when the smell source is placed in front of S3 we see its resistance fall while S1 is recovering and S2 is stationary, and finally when the smell source is placed close to S2 its resistance falls while the others are recovering. These experiments prove that the proposed nose provides not only information on the magnitude of the smell, but also its direction. We will use this information in the control strategies that we discuss in the next two sections.

III. Stationary Smell

A. Control strategy

In this section we present a smell driven control strategy for the task of reaching an odour source in the case of a smell whose concentration profile is constant over time. Based on the previously proved capability of our electronic nose to provide information about the direction of a smell location, we propose to exploit that information by computing iteratively a target in task space in the detected direction of the smell. It is reasonable to assume that the smell source will be in the premises of the sensor with highest reading at a given time. However this does not guarantee that the direction of the smell is precisely where that sensor is pointing. For this reason we consider the reading also of the second highest sensor and compute the vector of the new target, with respect to the center of the tip of the soft robot, as follows:

$$\overrightarrow{x}_{\text{target}} = k(G_1\overrightarrow{w_1} + G_2\overrightarrow{w_2}) \tag{1}$$

where $\overrightarrow{w_1}$ and $\overrightarrow{w_2}$ are the versors indicating the direction of the line joining the center of the soft robot to the two sensors with the highest readings in Ohms G_1 and G_2 respectively (Fig. 7). In this way the direction vector will be pointing more towards either one or the other sensor, based on the magnitude of their readings. The constant k is set to be inversely proportional to the the mean of all the sensor readings, in the current iteration: $k \propto (\frac{G_1+G_2+G_3}{3})^{-1}$. In this way the distance travelled by the robot towards the smell source at a given iteration will be greater when the source is far and smaller as the mean sensor reading rises, while the robot gets closer to the source. This process is done iteratively so that the robot can search for the smell source by moving along the detected direction of the incoming smell,

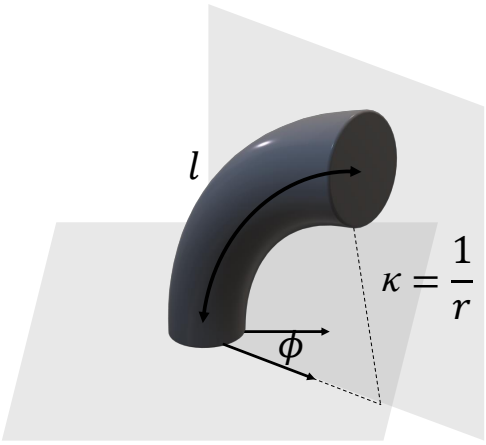

Fig. 6: Configuration space of the constant curvature segments constituting the PCC model with the main variables highlighted.

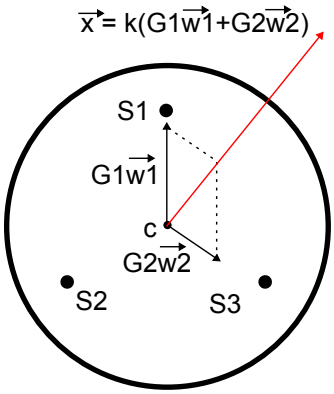

Fig. 7: The target computed by the proposed control strategy for stationary sells.

until the smell source is reached. The inverse kinematics of the soft robot is used to compute at every iteration the appropriate motor commands to reach the target. Since this strategy maps directly the magnitude of the sensor reading to the location of the odor source (1) it ignores dynamical properties of the smell. Therefore it is suitable for a situation where the smell concentration is constant over time. This method is proposed for cases where a constant smell source (e.g. a leak in a tank) is diffusing in an open space and it is reasonable to assume such profile to never become uniform over time due to the absence of spatial boundaries. Since this situation is hard to replicate in laboratory conditions, we have opted to validate the proposed strategies in simulation. Given the simple geometry of the soft robot at hand, a simple PCC model of the two segment soft robot was developed, with one CC segment per actuated segment. Referring to [20], we define the mapping from the actuator space (cable lengths) l to configuration space q as

$$s = \frac{l_1 + l_2 + l_3}{3},\ \phi = \text{atan2}\left(\frac{\sqrt{3}(l_2 + l_3 - 2l1)}{3(l_2 - l_3)}\right),$$
$$\kappa = \frac{2\sqrt{l_1^2 + l_2^2 + l_3^2 - l_1 l_2 - l_1 l_3 - l_2 l_3}}{d(l_1 + l_2 + l_3)}, \tag{2}$$

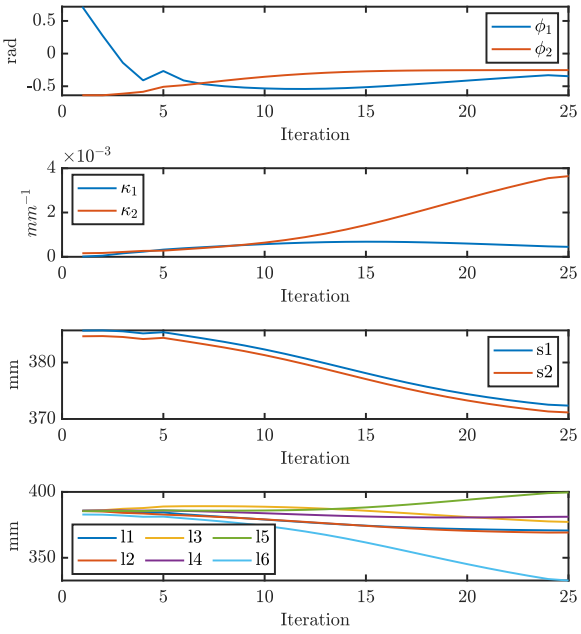

Fig. 8: Example of evolution over time of the configuration variables ϕ, κ, s for each simulated PCC segment and of the corresponding motor actions $l_{1...6}$.

where s is the arc length, κ the curvature, ϕ the rotation along the z axis as in Fig. 6, and d is the diameter of the section of the soft robot. The tendon lengths are l_1, l_2 and l_3. Using geometrical considerations [20], it is possible to derive the homogeneous transform T for every segment which provides the position and orientation of the tip of each segment with respect to its base. The multiplication of the two homogeneous matrices produces therefore the mapping from the robot's configuration space to its task space. The final homogeneous tranform and (2) constitute the forward kinematics of the robot: $\boldsymbol{x} = f_{\text{FK}}(\boldsymbol{L})$ where $\boldsymbol{L} = [l_1, ..., l_6]$ are the tendon lengths and $\boldsymbol{x}$ is the position of the robot's tip in Cartesian space. After computing the jacobian of the robot as

$$J = \left[\frac{\partial f_{\text{FK}}(l_1)}{\partial l_1}, ... \frac{\partial f_{\text{FK}}(l_6)}{\partial l_6}\right]^\top, \tag{3}$$

it is possible to compute the inverse kinematics of the soft arm by means of the pseudo inverse of the jacobian [21]:

$$\dot{\boldsymbol{L}} = J^+(\boldsymbol{L})(\boldsymbol{x}_{\textbf{target}} - f_{\text{FK}}(\boldsymbol{L})). \tag{4}$$

Solving (4) computes the appropriate motor actions to reach the target computed by (1), in every iteration.

B. Simulations

We have therefore modeled three ideal gas sensors placed on the tip of the soft arm, placed at a 120° degree angle. They act as if they sense exactly the gas concentration at a distance of 10 cm along the imaginary line which joins the center of the soft robot tip and the sensor. We assume that the maximum concentration of smell coincides with the

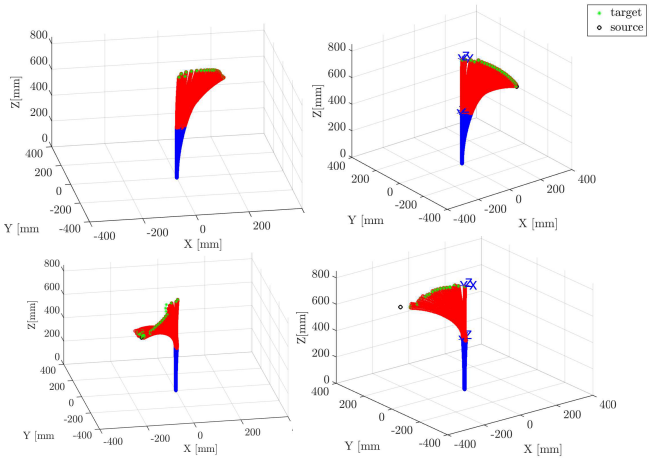

Fig. 9: Examples of trajectories of the simulated soft robot towards a stationary smell source, in different locations in space.

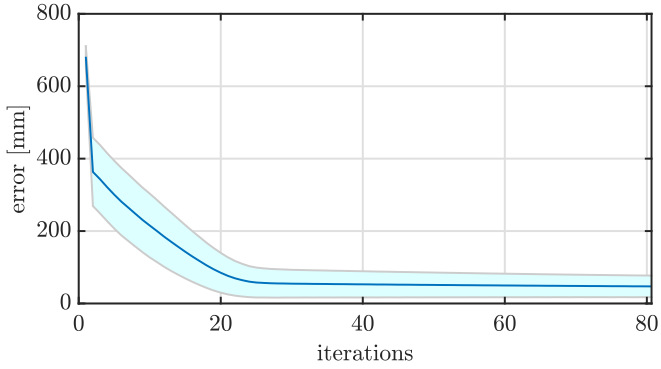

Fig. 10: Euclidean distance between the simulated robot's tip and the smell source, averaged over 1000 simulated trials, with $\sigma = 50$. We show the standard deviation band with a light blue shade area.

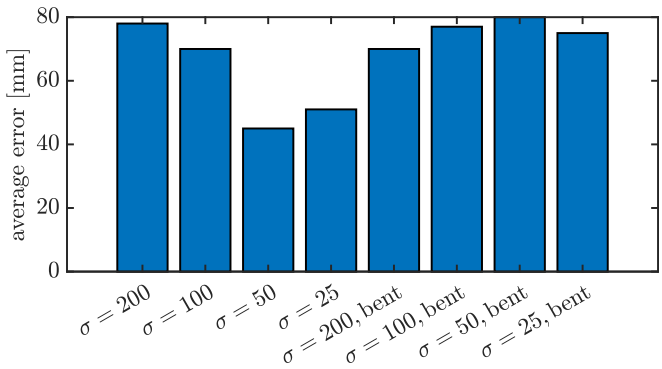

Fig. 11: The performance in terms of average final error of the proposed controller for different values of smell diffusion σ and for two different initial robot conditions.

smell source, and decreases as a Gaussian in function of the distance from the source. Therefore the reading of a given sensor in Cartesian space is given by:

$$G_n = \frac{1}{\sqrt{2\pi\sigma^2}} e^{\frac{-d_n}{2\sigma^2}} \tag{5}$$

Where d_n is the Euclidean distance between the sensor n and the smell source. By selecting the standard deviation σ of the Gaussian we are selecting how much the smell concentration is spread around the source, where the concentration is maximum. We simulate a soft robot using the aforementioned PCC model, and have it reach a stationary smell source using the proposed iterative algorithm: iterativaly a target is computed with (1) and the corresponding motor action, computed with (4), is fed into the PCC model (2). We repeat the trial 1000 times with the smell source placed in a different reachable point in the robot's workspace. We repeat this for varying values of σ, representing different levels of diffusion of the smell from the source, and for different initial conditions (straight and bent). The performance of the controller in terms of final reaching error in task space averaged over all the trials is shown in Fig. 11, for varying values of σ and of initial robot conditions. Examples of the trajectory of the robot in task space, reaching different smell targets are shown in Fig 9, while the evolution of the parameters of the PCC model, and of the tendons lengths are exemplified in Fig. 8. The average Euclidean distance of the simulated robot's tip with the smell source, along with its standard deviation, is shown in Fig. 10. We note that, for $\sigma = 50$ the robot reaches a smell source in different locations in less than 30 iterations, with a mean error of 45 mm, corresponding to about 5% of the robot's length.

IV. Dynamic Smell

We now consider the case in which the smell concentration is dynamic. This is the most common case in the lab, where the smell source appears in the scene, reaches the sensor in a given amount of time, and diffuses in the room. Local air currents or perturbations also influence the dynamics. Therefore in this section, we present a simple control strategy based on a one-to-one mapping of the sensors to the actuators. Such strategy will exploit the dynamics of the smell concentration so as to produce a reaching task towards a smell source, suitable for application in blind exploration. We then validate the strategy on the hardware.

A. Control strategy

We propose to directly couple the motors driving the tendons to the corresponding gas sensor, given that the three tendon attachment points on the tip are placed at a 120° angle corresponding to each gas sensor. Such topology is very common in the field of soft robotic manipulators [20]. Therefore this strategy applies to many soft tendon-driven robotic arms and beyond. The strategy consists in first reading raw gas sensor data, streamed by an Arduino to MATLAB at a frequency of 10 Hz. For each sensor the data is stored in a buffer to which a sliding window averaging

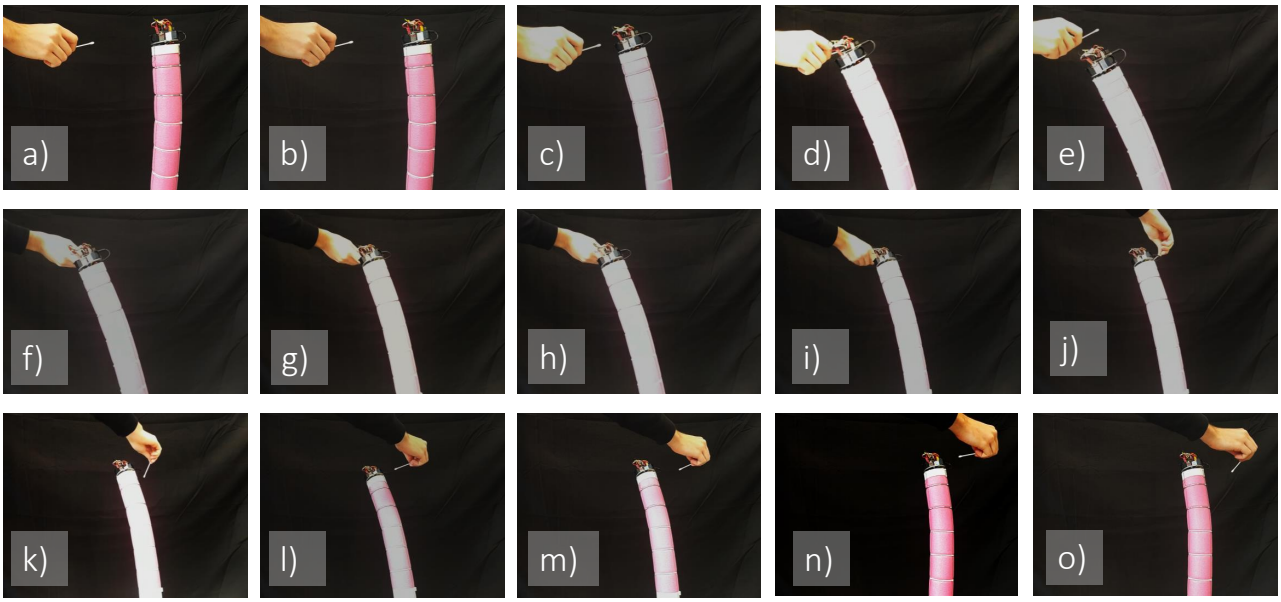

Fig. 12: Photo sequence of the soft robot following a smell source using the proposed strategy for dynamic smells. a) 0 s, b) 2.5 s, c) 4 s, d) 5 s, e) 7 s. f) 0 s, g) 2 s, h) 3 s, i) 4 s, j) 5 s. k) 0 s, l) 2 s, m) 4 s, n) 7 s, o) 8 s.

filter with a window of 10 samples is applied to smooth out the incoming data:

$$S_i = \frac{1}{10} \sum_{k=-10}^{1} S_{i-k+1,\text{raw}} \tag{6}$$

Where $S_{i,\text{raw}}$ and S_i are the raw sensor data and the smoothed data respectively, at time sample i. The gradient of the resulting signal was then computed using the `diff` command in MATLAB, and it was used to identify peaks of incoming smell concentration gradient.

$$S_{i,\text{diff}} = S_i - S_{i-1} \tag{7}$$

Such peaks are associated to the presence of the smell source in the premises of the corresponding sensor. Once the value of the smoothed and differentiated signal $S_{i,\text{diff}}$ overcomes a threshold, here imposed equal to 0.5, the corresponding motor is actuated with a step signal so that the tendon length is shortened of 5 mm. This was iteratively repeated every second. We summarise this control strategy in Algorithm 1.

Algorithm 1 Algorithm for reaching a dynamically varying smell

```
define thresh = 0.5
define action = 5 mm
while True do
    [S1, S2, S2] ← ReadSensors()
    Buffers ← Append([S1, S2, S3])
    Smoothed ← MovingAverage(Buffers)
    Diff ← diff(Smoothed)
    Flag ← Diff(end)
    if Flag_i > thresh then
        Motor_i ← action
    wait 1 s
```

B. Experimental results

To validate the proposed algorithm we have placed a smell source at a distance of about 10 cm from one of the sensors at the tip of the robot. Then, after the robot has reached the smell source and has stopped we have moved slowly the smell source around the workspace. The robot was able to follow the smell source accordingly (Fig. 12). The soft robot directs itself towards the smell source after the time needed for the smell to dynamically reach the sensors. In Fig. 13 the sensor readings recorded during the trial, the smoothed and differentiated signals used to trigger the motors, and the corresponding actuation signals in tendon lengths are shown. The smoothed and differentiated signal overcomes the threshold and activates the motors in three clearly separable moments, producing the three movements performed by the robot shown in Fig.12. This approach is advantageous since the motors are activated not only when the smell impacts the robot, but also while the robot approaches the smell source, since it is going towards a zone of higher smell concentration thus producing a gradient in sensor readings. This ensures the correct execution of a reaching task. Moreover, the proposed method effectively produces a stopping criterion for the robot due to the fact that when the tip is very near to the source the corresponding sensor saturates to the maximum reading. This results in a null gradient and therefore to the stopping of the motor. This approach has the advantage of being virtually applicable to any tendon driven soft robot, and of being simple to implement, since it does not require a kinematic inversion. However, for this same reason the path to the source is only

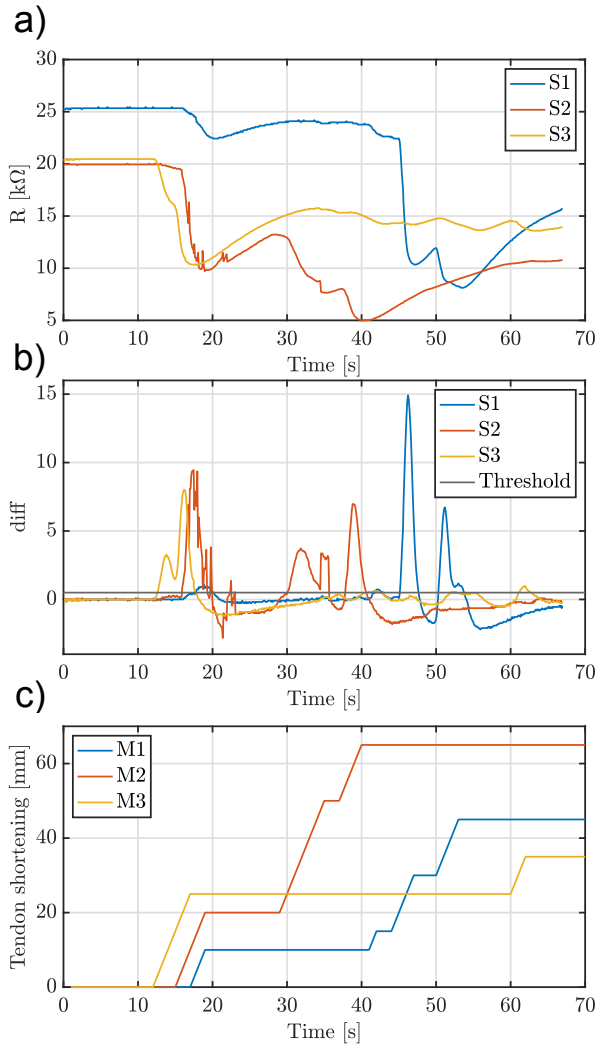

Fig. 13: a) Sensor resistances. b) Smoothed and differentiated raw signals from the sensors, shown with respect to the activation threshold. c) The corresponding motor actions.

approximate and does not span the whole workspace of the robot. Moreover, to respect the one-to-one mapping between sensors and actuators, in this work we have considered only the three actuators of the second segment which, due to heavy coupling between segments, produce a bending motion along all the robot's body. A strategy which considers also the actuators of the first segment would significantly improve the reachable workspace of the soft robot.

V. Conclusion

In this work we propose for the first time an artificial nose for a soft robotic arm. We present and validate two smell driven control strategies for two different conditions of smell diffusion. The first is to locate and reach a smell source with a stationary smell profile. We validated this strategy in simulation. The second controller considers a dynamic smell and was validated experimentally on the hardware. The results presented in this work are but the first step towards integrating olfactory sense in soft manipulators and using it for navigation, which could prove of great interest in the search and rescue field. Future studies will focus on strategies to locate robustly a smell source also in the case of smell concentration varying dynamically over time.

References

[1] S. Kim, C. Laschi, and B. Trimmer, "Soft robotics: a bioinspired evolution in robotics," *Trends in biotechnology*, vol. 31, no. 5, pp. 287–294, 2013.

[2] C. Della Santina, M. G. Catalano, and A. Bicchi, *Soft Robots*, pp. 1–15. Berlin, Heidelberg: Springer Berlin Heidelberg, 2021.

[3] J. M. Plotnik, R. C. Shaw, D. L. Brubaker, L. N. Tiller, and N. S. Clayton, "Thinking with their trunks: elephants use smell but not sound to locate food and exclude nonrewarding alternatives," *Animal Behaviour*, vol. 88, pp. 91–98, 2014.

[4] H. Wang, M. Totaro, and L. Beccai, "Toward perceptive soft robots: Progress and challenges," *Advanced Science*, vol. 5, no. 9, p. 1800541, 2018.

[5] S. Kamtikar, S. Marri, B. Walt, N. K. Uppalapati, G. Krishnan, and G. Chowdhary, "Visual servoing for pose control of soft continuum arm in a structured environment," *IEEE Robotics and Automation Letters*, vol. 7, no. 2, pp. 5504–5511, 2022.

[6] G. Fang, X. Wang, K. Wang, K.-H. Lee, J. D. Ho, H.-C. Fu, D. K. C. Fu, and K.-W. Kwok, "Vision-based online learning kinematic control for soft robots using local gaussian process regression," *IEEE Robotics and Automation Letters*, vol. 4, no. 2, pp. 1194–1201, 2019.

[7] J. L. Molnar, C.-A. Cheng, L. O. Tiziani, B. Boots, and F. L. Hammond, "Optical sensing and control methods for soft pneumatically actuated robotic manipulators," in *2018 IEEE International Conference on Robotics and Automation (ICRA)*, pp. 3355–3362, IEEE, 2018.

[8] G. Soter, A. Conn, H. Hauser, and J. Rossiter, "Bodily aware soft robots: integration of proprioceptive and exteroceptive sensors," in *2018 IEEE international conference on robotics and automation (ICRA)*, pp. 2448–2453, IEEE, 2018.

[9] T. G. Thuruthel, B. Shih, C. Laschi, and M. T. Tolley, "Soft robot perception using embedded soft sensors and recurrent neural networks," *Science Robotics*, vol. 4, no. 26, p. eaav1488, 2019.

[10] J. Hughes, F. Stella, C. D. Santina, and D. Rus, "Sensing soft robot shape using imus: An experimental investigation," in *International Symposium on Experimental Robotics*, pp. 543–552, Springer, 2020.

[11] L. Scimeca, J. Hughes, P. Maiolino, and F. Iida, "Model-free soft-structure reconstruction for proprioception using tactile arrays," *IEEE Robotics and Automation Letters*, vol. 4, no. 3, pp. 2479–2484, 2019.

[12] R. L. Truby, C. Della Santina, and D. Rus, "Distributed proprioception of 3d configuration in soft, sensorized robots via deep learning," *IEEE Robotics and Automation Letters*, vol. 5, no. 2, pp. 3299–3306, 2020.

[13] M. L. Preti, M. Totaro, E. Falotico, M. Crepaldi, and L. Beccai, "Online pressure map reconstruction in a multitouch soft optical waveguide skin," *IEEE/ASME Transactions on Mechatronics*, 2022.

[14] V. Wall, G. Zöller, and O. Brock, "Passive and active acoustic sensing for soft pneumatic actuators," *arXiv preprint arXiv:2208.10299*, 2022.

[15] K. Persaud and G. Dodd, "Analysis of discrimination mechanisms in the mammalian olfactory system using a model nose," *Nature*, vol. 299, no. 5881, pp. 352–355, 1982.

[16] T. Duckett, M. Axelsson, and A. Saffiotti, "Learning to locate an odour source with a mobile robot," in *Proceedings 2001 ICRA. IEEE International Conference on Robotics and Automation (Cat. No. 01CH37164)*, vol. 4, pp. 4017–4022, IEEE, 2001.

[17] H. Fan, E. Schaffernicht, and A. J. Lilienthal, "Ensemble learning-based approach for gas detection using an electronic nose in robotic applications," *Frontiers in chemistry*, vol. 10, 2022.

[18] M. A. Arain, V. Hernandez Bennetts, E. Schaffernicht, and A. J. Lilienthal, "Sniffing out fugitive methane emissions: autonomous remote gas inspection with a mobile robot," *The International Journal of Robotics Research*, vol. 40, no. 4-5, pp. 782–814, 2021.

[19] A. J. Lilienthal and T. Duckett, "Experimental analysis of smelling braitenberg vehicles," in *IEEE international conference on advanced robotics (ICAR 2003), Coimbra, Portugal, June 30-July 3, 2003*, vol. 1, pp. 375–380, Coimbra, University, 2003.

[20] R. J. Webster III and B. A. Jones, "Design and kinematic modeling of constant curvature continuum robots: A review," *The International Journal of Robotics Research*, vol. 29, no. 13, pp. 1661–1683, 2010.

[21] B. A. Jones and I. D. Walker, "Kinematics for multisection continuum robots," *IEEE Transactions on Robotics*, vol. 22, no. 1, pp. 43–55, 2006.